

ARTICLE OPEN



Glucocorticoid-glucocorticoid receptor-HCN1 channels reduce neuronal excitability in dorsal hippocampal CA1 neurons

Jiwon Kim¹, Yun Lei¹, Xin-Yun Lu¹ and Chung Sub Kim¹✉

© The Author(s) 2022

While chronic stress increases hyperpolarization-activated current (I_h) in dorsal hippocampal CA1 neurons, the underlying molecular mechanisms are entirely unknown. Following chronic social defeat stress (CSDS), susceptible mice displayed social avoidance and impaired spatial working memory, which were linked to decreased neuronal excitability, increased perisomatic hyperpolarization-activated cyclic nucleotide-gated (HCN) 1 protein expression, and elevated I_h in dorsal but not ventral CA1 neurons. In control mice, bath application of corticosterone reduced neuronal excitability, increased tetratricopeptide repeat-containing Rab8b-interacting protein (TRIP8b) and HCN1 protein expression, and elevated I_h in dorsal but not ventral CA1 region/neurons. Corticosterone-induced upregulation of functional I_h was mediated by the glucocorticoid receptor (GR), HCN channels, and the protein kinase A (PKA) but not the calcium/calmodulin-dependent protein kinase II (CaMKII) pathway. Three months after the end of CSDS, susceptible mice displayed persistent social avoidance when exposed to a novel aggressor. The sustained behavioral deficit was associated with lower neuronal excitability and higher functional I_h in dorsal CA1 neurons, both of which were unaffected by corticosterone treatment. Our findings show that corticosterone treatment mimics the pathophysiological effects of dorsal CA1 neurons/region found in susceptible mice. The aberrant expression of HCN1 protein along the somatodendritic axis of the dorsal hippocampal CA1 region might be the molecular mechanism driving susceptibility to social avoidance.

Molecular Psychiatry (2022) 27:4035–4049; <https://doi.org/10.1038/s41380-022-01682-9>

INTRODUCTION

Post-traumatic stress disorder (PTSD) is a debilitating long-term mental disease that can develop following exposure to traumatic, life-threatening events such as physical, emotional, or sexual attacks, natural disasters, wars, and pandemics [1]. Reliving the horrific incident, actively avoiding unpleasant memories or cues, negative mood and thoughts, such as emotional numbing and anhedonia, and hyperarousal, such as irritability, anger, hypervigilance, and sleep issues, are all symptoms of PTSD [1]. Individuals, families, and society face significant issues in terms of well-being, relationships, and financial burden due to these complex symptoms [2–4]. Additionally, those with PTSD are more likely to have comorbid conditions such as depression, anxiety, cardiovascular disease, and drug abuse disorder [5, 6], which increases the chance of attempting suicide [7, 8]. One of the most common symptoms of PTSD is avoidance. Experiential avoidance is defined as attempts to avoid private traumatic experiences (i.e., thoughts, feelings, memories, physical sensations), even if doing so causes long-term harm [9]. A growing body of literature suggests that experiential avoidance is the key diagnostic feature of PTSD [10–13].

Animal models are critical for researching the pathophysiology of PTSD because they allow researchers to track the development of PTSD over time using controlled stresses. It is worth noting that it only affects a small percentage of persons who have been exposed to potentially fatal events. Chronic social defeat stress (CSDS) is a psychosocial stress animal model that causes PTSD symptoms like social avoidance, emotional shifts, and anxiety-like behavior [14].

CSDS produces interindividual variation (i.e., susceptible and resilient phenotypes) [14], similar to that seen in patients with PTSD. This animal model is a valuable resource for understanding the mechanisms underlying the development of susceptibility and resilience to social avoidance.

Functional neuroimaging of PTSD patients reveals structural and functional changes in the hippocampus, amygdala, and medial prefrontal cortex [15–17]. In PTSD patients [18–20], researchers found that decreased hippocampal volume, hypoactivity of the hippocampus, and disruption of the hypothalamic–pituitary–adrenal (HPA) axis. The hippocampus is a critical brain region in PTSD symptoms such as spatial working memory and emotion-related behavior [18, 21]. The hippocampus, which includes high amounts of mineralocorticoid receptor and GR, regulates HPA-axis activity among limbic brain structures [22]. Cortisol levels in PTSD patients are higher than in the healthy control group when they re-experience stressful situations [23–25]. Administration of exogenous glucocorticoids has been linked to decreased memory performance in healthy people [26, 27]. Animals treated with corticosterone or repeated stress impair spatial working memory [28, 29]. The hippocampus of rodents can be separated anatomically and functionally into two brain regions: the dorsal hippocampus, which corresponds to the human posterior hippocampus, and the ventral hippocampus, which corresponds to the human anterior hippocampus [30, 31]. The dorsal hippocampus is mainly linked to spatial learning and memory, while the ventral hippocampus is associated with emotion-related reactions like anxiety [31–33]. Furthermore, dorsal and ventral CA1 regions of the

¹Department of Neuroscience & Regenerative Medicine, Medical College of Georgia at Augusta University, Augusta, GA 30912, USA. ✉email: ckim5@augusta.edu

Received: 4 February 2022 Revised: 15 June 2022 Accepted: 27 June 2022

Published online: 15 July 2022

hippocampi have distinct electrophysiological properties. Compared to ventral CA1 neurons, dorsal CA1 neurons have a hyperpolarized resting membrane potential, lower input resistance, and reduced neuronal excitability [34].

HCN channels generate membrane currents that are characterized by (1) cyclic nucleotide-mediated modulation, (2) Na^+ and K^+ permeability, and (3) activation by membrane hyperpolarization [35]. HCN1 is the major isoform expressed in the hippocampus, neocortex, and cerebellar cortex, although there are four isoforms of HCN channels (HCN1–HCN4) [36, 37]. In the hippocampal CA1 region, HCN1 expression displays a gradient of increasing channel density along the somatodendritic region of CA1 [38, 39]. A portion of HCN channels is active at resting membrane potential, resulting in a non-inactivating inward current that affects intrinsic membrane properties, neuronal excitability, synaptic integration, and synaptic plasticity [40]. Evidence suggests a link between HCN channels and mental diseases, including depression and anxiety [41–46]. Whole-brain knockout mice lacking either the pore-forming protein (HCN1 and HCN2) or an auxiliary channel subunit, tetratricopeptide repeat-containing Rab8b-interacting protein (TRIP8b), exhibit antidepressant-like behaviors [41]. Normal rats demonstrate antidepressant- and anxiolytic-like effects when HCN1 protein is lowered in the dorsal but not ventral CA1 area [42]. Rats exposed to chronic unpredictable stress (CUS) for two to four weeks show depressive- and anxiogenic-like behaviors associated with the upregulation of perisomatic I_h in the dorsal but not ventral CA1 region/neurons [43, 44]. These findings imply that chronic stress, but not acute stress, causes pathogenic alterations in CA1 neurons in the dorsal but not ventral hippocampi. The molecular mechanisms driving pathogenic changes in I_h , on the other hand, are unknown.

This study found that CSDS produced susceptible and resilient phenotypes during the social interaction test. Although both susceptible and resilient mice showed anxiogenic-like behavior during the elevated plus-maze test, spatial working memory was impaired in susceptible mice compared to control and resilient mice in the Y maze spontaneous alternation test. Compared to control and resilient mice, dorsal but not ventral CA1 neurons had lowered input resistance (R_{in}) and reduced neuronal excitability. In susceptible mice, perisomatic HCN1 protein expression and I_h were elevated in the dorsal but not ventral CA1 neurons/region, indicating increased functional I_h (i.e., decreased R_{in} and neuronal excitability). In control mice, bath application of corticosterone reduced R_{in} and decreased neuronal excitability in the dorsal but not ventral CA1 neurons. We further found that corticosterone pretreatment increased I_h as well as TRIP8b and HCN1 protein expression in the perisomatic CA1 region/neurons of the dorsal hippocampus. Corticosterone-induced functional I_h was mediated by the GR, HCN channels, and the PKA but not the CaMKII pathway. Susceptible mice were reintroduced to novel aggressor mice one month or three months after the end of the CSDS and displayed persistent social avoidance. This long-term behavioral impairment was linked to decreased neuronal excitability, increased TRIP8b and HCN1 protein expression, and elevated I_h in the dorsal CA1 region/neurons. On the other hand, resilient mice displayed increased neuronal excitability in the dorsal CA1 neurons. Corticosterone had no additional impacts on functional I_h in the dorsal CA1 neurons from susceptible mice, but it did in control and resilient mice. Our findings show that functional I_h may be involved in cellular pathways that drive the development of susceptibility and resilience to social avoidance.

MATERIALS AND METHODS

Animals

Male wild-type C57BL/6J mice (7 to 16 weeks old) were used in this study. Mice were housed 5 per cage on a 12 h light schedule (on 7:00 A.M. off 7:00 P.M.) with ad libitum access to water and food. In a study with one

month or three months without CSDS, mice were single-housed following CSDS. All procedures involving animals were approved by the Institutional Animal Care and Use Committee of Augusta University.

Drugs

Corticosterone (Cat # 3685), dexamethasone (Cat # 1126), mifepristone (RU 486; Cat # 1479), KT5720 (Cat #1288), KN-62 (Cat #1277), and ZD7288 (Cat #1000) were purchased from Tocris. Corticosterone, Dexamethasone, KT5720, and KN-62 were dissolved in dimethyl sulfoxide and diluted to a final concentration in artificial cerebral spinal fluid (aCSF).

Chronic social defeat stress

Social defeat was generated using a resident–intruder paradigm with minor modifications [47]. 3-to-4-month-old male CD-1 mouse was co-housed with ovariectomized female CD-1 mouse for at least two weeks. Subsequently, male sexually experienced CD-1 mice (residents) were housed individually for one week before being screened for aggression. During the screening process, a ‘screener’ C57BL/6J mouse was introduced into the cage of a singly housed CD-1 mouse for 3 min/session/day and the latency of the CD-1 mouse to attack the ‘screener’ C57BL/6J mouse during each session was recorded. The screening procedure was repeated for three consecutive days. The male CD-1 mice with the attack latency <60 s for at least two sessions on the last day were selected for aggressors in social defeat experiments. For the chronic social defeat procedure, male C57BL/6J experimental mice were individually introduced into the large home cage of an aggressor CD-1 mouse for 5 to 15 min during which time the experimental mouse was physically and emotionally defeated. After 5 to 15 min aggression encounter session, the CD-1 aggressor mouse and the experimental C57BL/6J mouse were housed together but separated by a perforated Plexiglass divider to allow sensory contact for the remainder of the 24-h period. The following day, the experimental C57BL/6J mice were re-exposed to a new CD-1 aggressor mouse for 5–15 min of direct physical contact and then a 24-h period of emotional contact. The procedure was repeated for 12 days total. Control C57BL/6J mice were housed two per cage in the cages identical to those used for socially defeated mice. After the last social defeat stress, control and defeated mice were individually housed in standard cage. Selection of aggressors and social defeat stress were performed between 4 pm and 6 pm.

Behavioral experiment

All behavioral measurements were analyzed by custom-written programs. All behavioral experiments were performed between 4 pm and 6 pm. All experiments were performed under blind conditions.

Social interaction test

Social interaction test was assessed at 48 h after the last social defeat stress session. Mice were acclimated to a behavior room under red-light conditions (~4 lux) for at least 1 h. The apparatus is made of a box (18 × 18 × 12 in) with a perforated Plexiglass cage (4 × 4 × 12 in) at the middle of one side of the box. The social interaction test consisted of a two-trial procedure under red-light conditions (~4 lux). The experimental mice were placed in the corner of the open arena and allowed to freely explore for 2.5 min (i.e., 1st session without social target). After the 1st session, an unfamiliar CD1 male mouse was introduced into the perforated Plexiglass cage as a social stimulus for 2.5 additional min (i.e., 2nd session with social target). The surface of the open field was cleaned with 70% EtOH in order to remove permeated odors by previous animals after each trial. A CCD camera placed above the apparatus recorded behavior. A social interaction ratio was calculated as the ratio of the time spent in the interaction zone in the presence of a social target to the time spent in the interaction zone without a social target. Mice with scores more than 1 were defined as “resilient” and those with scores less than 1 were defined as “susceptible” [47].

Elevated plus-maze test

Anxiety was tested on the elevated plus-maze apparatus described previously [43]. The apparatus is made of a black acrylic sheet. Four arms (12 in long and 3 in wide) are connected and elevated to a height of 16 in from the floor. Mice were placed on the central platform facing an open arm and allowed to explore the maze for 6 min. The surface was cleaned with 70% EtOH to remove permeated odors by previous animals after each trial. Behavior in the elevated plus maze was recorded for 6 min using a

CCD camera. The time spent in the open arm and the number of total arm entries were determined. Arm entry was defined as 50% of the body being positioned within the arm.

Y maze spontaneous alternation test

Short-term spatial working memory was examined using the Y maze spontaneous alternation test as previously described [28]. The apparatus consists of three identical arms (each arm: 14 in x 3 in; no intra-maze cues) diverging at 120° angle from each other. In the Y maze, there is no blocking off of each arm. The mice were placed in the one arm of the Y maze (start arm) and allowed to freely explore the arena for 6 min. The sequence of arm entries and the total number of arm entries were measured. The surface of the maze was cleaned with 70% EtOH in order to remove permeated odors by previous animals after each trial. A CCD camera placed above the apparatus recorded behavior. Arm entry is defined as having all four paws in the arm. An alternation is defined as successive entry into three different arms, on overlapping triplet sets. The percentage of alternations was calculated as the number of actual alternations divided by the maximum number of alternations (the total number of arm entries minus 2).

Acute hippocampal slice preparation

Mice were anesthetized with a lethal dose of isoflurane (>5%) in a closed plastic container and transcardially perfused with ice-cold aCSF composed of (in mM): 2.5 KCl, 1.25 NaH₂PO₄, 25 NaHCO₃, 0.5 CaCl₂, 7 MgCl₂, 7 dextrose, 210 sucrose, 1.3 ascorbic acid, and 3 sodium pyruvate, bubbled with 95% O₂ – 5% CO₂. The brain was removed and hemisected along the longitudinal fissure. Dorsal (coronal section with an angle of 10–20°) and ventral (horizontal section) hippocampal slices were prepared as previously described [43]. Hippocampal slices (300 μm thick) were made in ice-cold aCSF using a vibrating microtome (Microslicer DTK-Zero1, DSK, Kyoto, Japan). Slices were placed in a holding chamber containing (in mM) 125 NaCl, 2.5 KCl, 1.25 NaH₂PO₄, 25 NaHCO₃, 2 CaCl₂, 2 MgCl₂, 12.5 dextrose, 1.3 ascorbic acid, and 3 sodium pyruvate, bubbled with 95% O₂ – 5% CO₂ at 35 °C for 30 min and then incubated for at least 45 min at room temperature before used for electrophysiology.

Whole-cell patch-clamp recordings

Whole-cell current-clamp recordings were performed as previously described [34, 42, 43]. Briefly, hippocampal slices were submerged in a recording chamber continuously perfused with aCSF containing (in mM) 125 NaCl, 3 KCl, 1.25 NaH₂PO₄, 25 NaHCO₃, 2 CaCl₂, 1 MgCl₂, and 12.5 dextrose, bubbled with 95% O₂ – 5% CO₂ at a rate of 1 ml/min and 31–33 °C. For whole-cell voltage-clamp recordings, dorsal hippocampal slices were transferred to the recording chamber and perfused with aCSF containing (in mM) 125 NaCl, 3 KCl, 1.25 NaH₂PO₄, 25 NaHCO₃, 2 CaCl₂, 1 MgCl₂, and 12.5 dextrose, 1 BaCl₂, 10 TEA-Cl, 0.2 3,4-DAP bubbled with 95% O₂ – 5% CO₂ at a rate of 1 ml/min and 31–33 °C. CA1 pyramidal neurons were visually identified using a microscope (Olympus BX51WI, US) fitted with differential interference contrast optics [48]. Patch pipettes for somatic (4–7 MΩ) were prepared with capillary glass (external diameter 1.65 mm and internal diameter 1.1 mm, World Precision Instruments) using a Flaming/Brown micropipette puller (P-1000, Sutter Instrument, CA) and filled with an internal solution containing (in mM) 120 K-gluconate, 20 KCl, 10 HEPES, 4 NaCl, 7 K₂-phosphocreatine, 4 Mg-ATP, 0.3 Na-GTP (pH 7.3 with KOH). Whole-cell recordings were performed using a MultiClamp 700B amplifier (Molecular Devices, LLC, CA) and commercial acquisition software pCLAMP10 (Molecular Devices, LLC, CA). Electrical signals were filtered at 10 kHz, sampled at 20 kHz, and digitized by Axon Digidata 1440 A (Axon Instruments). For whole-cell current-clamp recordings, series resistance was monitored during each experiment and experiments were discarded if the series resistance exceeded 30 MΩ for somatic recordings. The resting membrane potential was the potential of the soma in the absence of any injected current. Liquid junction potential was not corrected and was estimated to be about –13 mV using the Patcher's Power Tools add-on in Igor Pro.

Cell-attached patch-clamp recordings

Cell-attached voltage-clamp recordings were performed as previously described [43, 44]. Pipettes contained the following (in mM): 120 KCl, 10 HEPES, 2.0 CaCl₂, 1.0 MgCl₂, 20 TEA-Cl, 0.2 3,4-DAP, 1 BaCl₂, pH 7.3 with KOH. Membrane currents were recorded using a MultiClamp 700B amplifier (Molecular Devices, LLC, CA) and commercial acquisition software pCLAMP10 (Molecular Devices, LLC, CA). Electrical signals were sampled at 10 kHz, analog filtered at 2 kHz by using Axon Digidata 1440 A (Axon Instruments). Maximal I_h was measured by using hyperpolarizing

voltage commands to –140 mV from a holding potential of –30 mV. Linear leakage and capacitive currents were digitally subtracted by scaling traces at smaller command voltages in which no voltage-dependent current was activated.

DAB staining

Neuronal reconstructions were performed as previously described [43]. Briefly, slices containing neurobiotin-filled neurons were fixed in a 3% glutaraldehyde solution (0.1 M phosphate buffer, pH 7.4) and stored at 4 °C before undergoing histological processing using an avidin-HRP system activated by diaminobenzidine (DAB; Vector Laboratories). DAB-processed slices were mounted in glycerol and viewed with a microscope (Revolve, ECHO). Images of the cell were created from z-stacks of photos taken at 10X under a microscope. The location of patched CA1 neurons in the dorsal and ventral hippocampus were determined. Experiments were performed under blind conditions.

Immunohistochemistry

Immunohistochemistry was carried out as described previously [42, 43]. 300 μm thick slices were further sectioned using a freezing microtome into 50-μm thin sections and stored in cryoprotectant (30% sucrose, 30% ethylene glycol, 1% polyvinyl pyrrolidone, 0.05 M sodium phosphate buffer). Sections were briefly rinsed in PBS buffer and incubated in 0.1% TritonX-100 for 30 min. Subsequently, slices were blocked in PBS solution containing 5% normal goat serum, 0.03% TritonX-100 for 1 h, and then incubated in primary antibody diluted in blocking solution overnight at 4 °C. Slices were rinsed in PBS buffer and then incubated in secondary antibody for 1 h at room temperature. Primary antibody in this study was used as follows; rabbit anti-HCN1 (1:500, Invitrogen, Cat # PA5-78675), rabbit anti-HCN2 (1:500, Invitrogen, Cat # PA1-918), rabbit anti-HCN3 (1:500, Invitrogen, Cat # PA5-104434), rabbit anti-HCN4 (1:500, Invitrogen, Cat # PA5-111793), rabbit C-terminal TRIP8b (1:500, Proteintech, Cat #13084-1-AP), and rabbit anti-GR (1:500, Invitrogen, Cat # PA1-511A). Experiments were performed under blind conditions.

Western blotting

Western blotting was carried out as previously described [42, 43]. After hippocampal acute slices, the dorsal CA1 region was isolated using 26-gauge needles under a dissecting microscope on ice. Isolated dorsal CA1 tissue was stored at –80 °C until processing for western blotting. The protein was separated on 10% sodium dodecyl sulfate-polyacrylamide gel and transferred to nitrocellulose membrane (Invitrogen). The membrane was incubated with blocking solution (LI-COR) for 1 h at room temperature and then with the primary antibody (rabbit anti-HCN1 1:500, Invitrogen; rabbit anti-GR 1:500, Invitrogen; mouse anti-β-tubulin 1:2000, Sigma-Aldrich) overnight at 4 °C. The membrane was rinsed in PBST buffer (0.05% Tween 20) 3 × 10 min, and then incubated in secondary antibody (LI-COR) for 1 h at room temperature. Experiments were performed under blind conditions.

Data analysis

Input resistance was measured by the slope of the linear fit of the V-I plot between +30 and –150 pA current injections. Single action potentials (APs) were analyzed for AP threshold, AP amplitude, AP half-width, and maximum *dv/dt* (mV/msec). AP threshold was defined as the voltage where *dv/dt* of the spike crossed 20 mV/ms. AP amplitude was determined from threshold to peak, with the half-width measured at half this distance.

Statistical analysis

Statistical comparisons were performed using ANOVA (one-factor or two-factor) followed by Bonferroni post-hoc test, paired *t*-test (Wilcoxon signed-rank test) or unpaired *t*-test (Mann-Whitney *U* test) with GraphPad software. The results of all statistical analyses were compiled into an word file. **P* < 0.05 was considered as statistically significant.

RESULTS

Susceptible mice displayed social avoidance and impaired spatial working memory

We used male mice aged 6 to 7 weeks and subjected them to CSDS for 12 days. (Figs. 1A and S1A). Mice were tested in the social interaction test, which assesses social avoidance, to see if CSDS

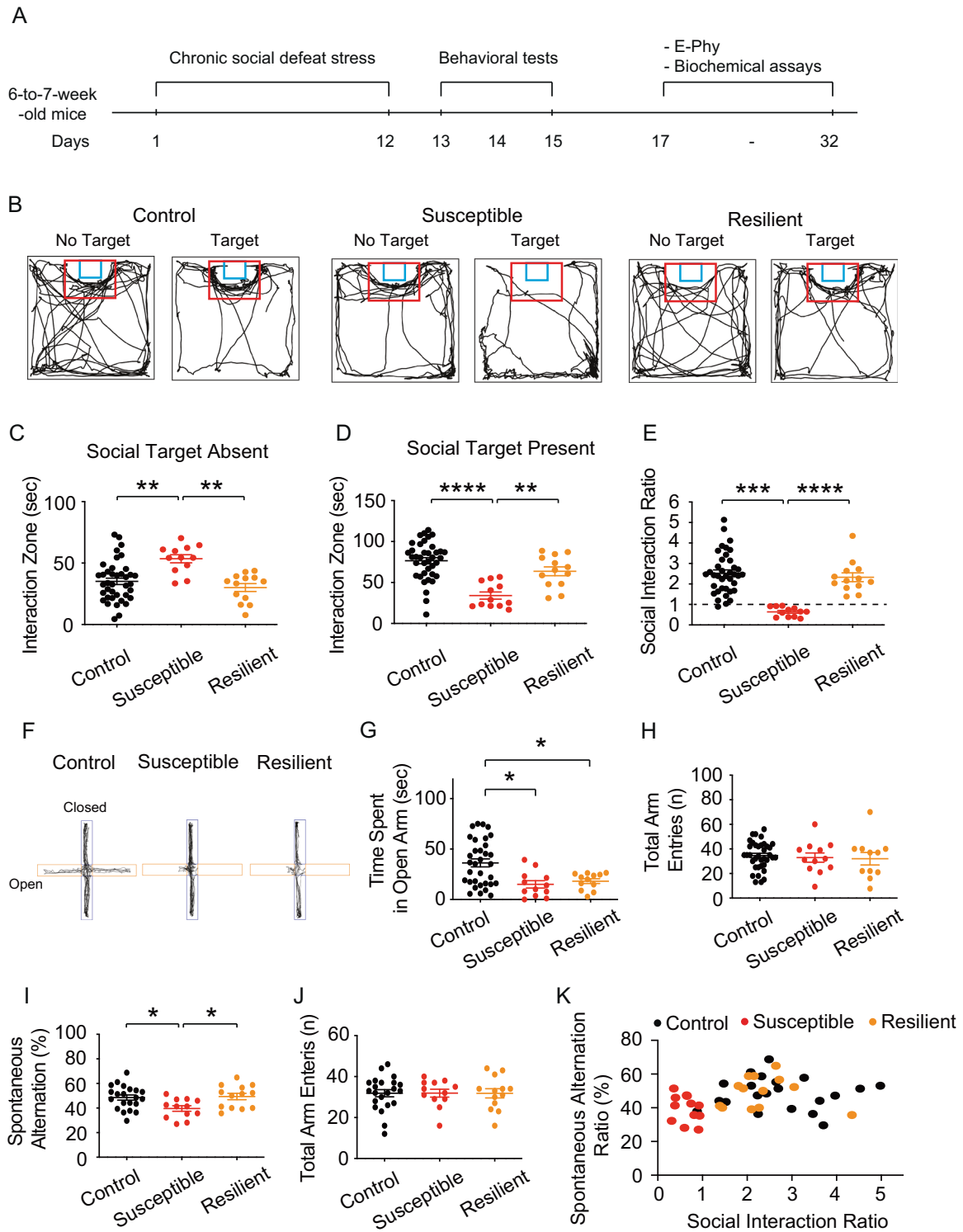


Fig. 1 Susceptible mice displayed social avoidance and impaired spatial working memory. **A** Timeline of chronic social defeat stress, behavioral tests, electrophysiology, and biochemical assay. **B** Representative video tracking images of control, susceptible, and resilient mice without and with a social target during the social interaction test. **C** In the absence of the social target, susceptible group spent more time in the interaction zone than the control and resilient groups. **D** In the presence of a social target, susceptible group spent less time in the interaction zone than the control and resilient groups. **E** During the social interaction test, chronic social defeat stress resulted in the formation of susceptible and resilient phenotypes. **F** Representative video tracking images of age-matched mice during a 6-min elevated plus maze test. **G, H** The susceptible and resilient groups spent less time in the open arm than the control group without changing the total arm entries. **I, J** The percentage of spontaneous alternation in susceptible group was much lower than in the control and resilient groups, despite no differences in total arm entries. **K** The relationship between social avoidance and spatial working memory between groups. Data are expressed as mean \pm SEM.

affected social behavior [49]. When CSDS-treated mice were not exposed to a novel conspecific, they spent a similar amount of time in the interaction zone as the control group. (Fig. S1C). CSDS-treated mice spent less time in the interaction zone than control mice when a new conspecific was brought into the cage as a social stimulus (Fig. S1D). Based on their social interaction ratio (Fig. S1F), CSDS-treated mice were separated into susceptible and resilient subgroups [14]. Susceptible mice spent more time in the interaction zone than control and resilient mice in the absence of a novel conspecific (Fig. 1B, C). In the presence of a novel conspecific, susceptible mice spent less time in the interaction zone than control and resilient mice (Fig. 1B, D). We found that CSDS could produce both susceptible and resilient phenotypes (Fig. 1E). The anxiety levels of the control and CSDS-treated groups were subsequently assessed using an elevated plus-maze test (Fig. 1A) [50]. Both susceptible and resilient mice spent less time in the open arm than the control group, but there was no difference in the overall number of arm entries (Fig. 1F, G). Hippocampal dysfunction is a crucial contributor to PTSD symptoms such as working memory [51, 52]. We further evaluate the spatial working memory of these animals using the Y maze spontaneous alternation test (Y maze test). The Y maze test is a frequently used method for assessing spatial learning and memory in mice by monitoring their propensity to explore novel surroundings [53]. In comparison to the control and resilient mice, susceptible mice demonstrated a lower percentage of spontaneous alternation (Fig. 1I) but no differences in total arm entries (Fig. 1J). The relationship between social avoidance and spatial working memory can be distinguished between susceptible and control or resilient mice (Fig. 1K).

Susceptible mice had a decrease in neuronal excitability of dorsal but not ventral CA1 neurons

Since susceptible mice displayed social avoidance and impaired spatial working memory, we used somatic whole-cell current-clamp recordings to see if the electrophysiological properties of hippocampal CA1 neurons were changed. Acute dorsal and ventral hippocampal slices were prepared after behavioral tests [43]. We put aside tissue samples for western blotting (i.e., cut the CA1 region) and immunohistochemistry after acute hippocampal slices. As a result, we can correlate electrophysiological data with protein expression. The resting membrane potential of dorsal CA1 neurons did not differ across groups (Fig. 2A, B). R_{in} of dorsal CA1 neurons was considerably lower in susceptible mice compared to the control and resilient mice at resting membrane potential (RMP) (Fig. 2C) and at -65 mV (Fig. S2A, B). The number of action potentials at RMP in dorsal CA1 neurons from susceptible mice was significantly lower than in the control and resilient mice (Fig. 2D, E), implying a reduction in neuronal excitability. We observed increased afterhyperpolarization from trains of action potentials of susceptible-dorsal CA1 neurons (data not shown), consistent with a reduction in neuronal excitability (Fig. 2D, E). RMP (Fig. 2F, G), R_{in} at RMP (Fig. 2F, H), R_{in} at -65 mV (Fig. S2C, D), and the number of action potentials at RMP (Fig. 2I, J), on the other hand, were not different across groups in ventral CA1 neurons. Because the number of action potentials at RMP was reduced in dorsal CA1 neurons from susceptible mice compared to the control and resilient mice, we examined the properties of a single action potential. In dorsal and ventral CA1 neurons, there were no differences in action potential threshold, half-width, amplitude, and max dv/dt between control, susceptible, and resilient groups (Supplementary Table 1). Since the magnitude of R_{in} is dependent on the longitudinal position of neurons in the CA1 region [54, 55], CA1 neurons were filled with neurobiotin during electrophysiological recordings and fixed for post-hoc morphological examination. There were no significant differences in the positions of recorded dorsal CA1 (Fig. S3A–C) and ventral CA1 (Fig. S3D–F) neurons across groups.

Susceptible mice had increased HCN1 protein expression and elevated I_h in dorsal CA1 region/neurons

HCN channels at RMP play an important role in intrinsic membrane properties including R_{in} [34]. We examined to see if HCN protein was altered in the hippocampal CA1 region. We used a 50 μ m thick resection from 300 μ m thick slices for immunohistochemistry. Indeed, HCN1 protein expression was considerably increased in the perisomatic CA1 region of the dorsal (Fig. 3A, B) but not ventral (Fig. 3C, D) hippocampus in susceptible but not control or resilient mice. Because other HCN channel subunits are also expressed in the hippocampus, we examined whether they were altered in susceptible mice. None of the HCN channel subunits, on the other hand, were different across the groups (Fig. S4A–L). Furthermore, HCN1 protein expression in dorsal CA1 region was significantly greater in susceptible mice compared to the control and resilient mice (Fig. 3E). We then measured I_h at the soma of dorsal CA1 neurons using cell-attached patch-clamp recordings. After subtracting linear leakage and capacitive currents by scaling traces at -40 mV, the h current exhibited a lack of time-dependent component of I_h in response to voltage, as shown in Fig. 2A, F voltage traces. Patches from susceptible mice exhibited significantly higher I_h than patches from the control and resilient mice (Fig. 3F, G), which was consistent with increased HCN1 protein expression. Consistent with the cell-attached recordings, whole-cell voltage-clamp recordings revealed that I_h was significantly increased in the dorsal CA1 neurons of susceptible group compared to control or resilient group (Fig. 3H, I). We further found that the half-activation voltage ($V_{1/2}$) of the h channel activation curve for susceptible group was significantly shifted to the right by around $+10$ mV ($V_{1/2}$ of control: -101.8 mV; susceptible: -90.02 mV; resilient: -102.1 mV, Fig. 3J, K), whereas the slope factor was not different (Fig. 3J, L) compared to control and resilient groups.

Dorsal CA1 neurons showed greater response to corticosterone than ventral CA1 neurons

Dysregulation of the HPA axis is common in people with severe mental illness including PTSD [56, 57]. When glucocorticoid levels are high, GR-expressing neurons in the hippocampus [58] and the hypothalamus [59], which have a low affinity for corticosterone, are likely to be the main target for negative feedback [60]. We, therefore, examined the expression of GR in the hippocampus using immunohistochemistry and western blotting in control mice. GR protein was shown to be more abundant in the perisomatic CA1 region of dorsal hippocampus than ventral hippocampus (Fig. 4A–C). Consistent with this result, GR protein expression in dorsal CA1 region was significantly higher than in ventral CA1 region (Fig. 4D). It has been reported that a bath application of 100 nM corticosterone for 20 min is sufficient to occupy GRs in hippocampal CA1 neurons, resulting in increased Ca^{2+} current amplitude, which was prevented by pretreatment with the GR antagonist [61, 62]. We previously reported that in vitro or in vivo block of the sarcoplasmic/endoplasmic reticulum Ca^{2+} -ATPase (SERCA) pumps in CA1 neurons increases perisomatic I_h [43, 44, 63]. Given that dorsal CA1 region had more GR expression than ventral CA1 region, we investigated if corticosterone had distinct physiological effects on CA1 neurons in dorsal and ventral hippocampi. Corticosterone had physiological effects (e.g., changes in R_{in} and the number of action potentials) after 20 min, and the effects were reversible over time (Data not shown). We, therefore, treated corticosterone for 20 min in all our experiments. In dorsal CA1 neurons, corticosterone had no effect on RMP (Fig. 4E, F), but lowered R_{in} at RMP (Fig. 4E, G) and at -65 mV (Fig. S5A, B) compared with baseline. Furthermore, the number of action potentials elicited by depolarizing current steps at RMP (Fig. 4K, L) and at -65 mV (Fig. S5E, F) was significantly decreased compared with baseline. However, there were no significant differences in RMP (Fig. 4H, I), R_{in} at RMP (Fig. 4H, J) and at -65 mV (Fig. S5C, D), and the number of action potentials at RMP (Fig. 4M, N) and at -65 mV (Fig. S5G, H) in ventral CA1 neurons before and after treatment with 100 nM corticosterone. Although corticosterone at a concentration of

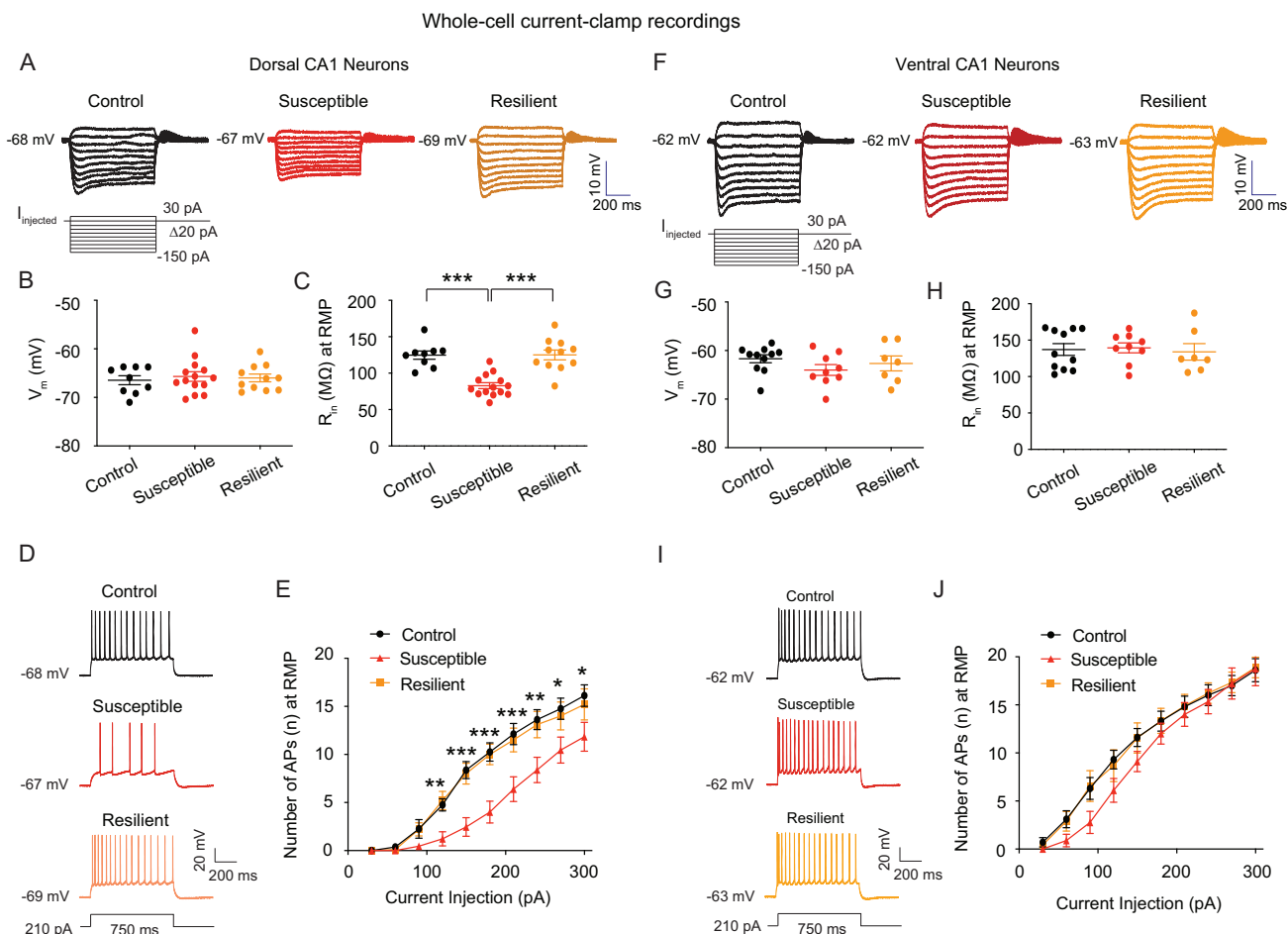


Fig. 2 The susceptible group reduced R_{in} and neuronal excitability in dorsal CA1 neurons, but not in ventral CA1 neurons. A–J We performed whole-cell current-clamp recordings. **A** Representative voltage responses with step current commands ranging from -150 pA to $+30$ pA ($\Delta = 20$ pA) at RMP. **B** There was no difference in RMP of dorsal CA1 neurons between groups. **C** The dorsal CA1 neurons of the susceptible group had lower R_{in} at RMP than the control and resilient groups. **D** Representative voltage responses with depolarizing current step (210 pA; 750 ms) at RMP in dorsal CA1 neurons from the control, susceptible, and resilient groups. **E** Dorsal CA1 neurons from susceptible group had lower action potential firing than the control and resilient groups. **F** Representative voltage responses with step current commands ranging from -150 pA to $+30$ pA ($\Delta = 20$ pA) at RMP. **G, H** There were no differences in RMP and R_{in} at RMP of ventral CA1 neurons between groups. **I** Representative voltage responses with depolarizing current step (210 pA; 750 ms) at RMP in the ventral CA1 neurons from the control, susceptible, and resilient groups. **J** Action potential firing of ventral CA1 neurons was not different between groups. Data are expressed as mean \pm SEM.

100 nM had different physiological effects on hippocampal CA1 neurons, we wondered if other corticosterone concentrations did as well. We then examined the same electrophysiological parameters (i.e., R_{in} and APs) with different concentrations of corticosterone (i.e., 10 nM and 1 μ M). We found that neither 10 nM corticosterone (Fig. S6A, J) nor 1 μ M corticosterone (Fig. S7A, J) had effects on dorsal or ventral CA1 neurons (Fig. 4O–Q). We, therefore, used 100 nM corticosterone for all our experiments.

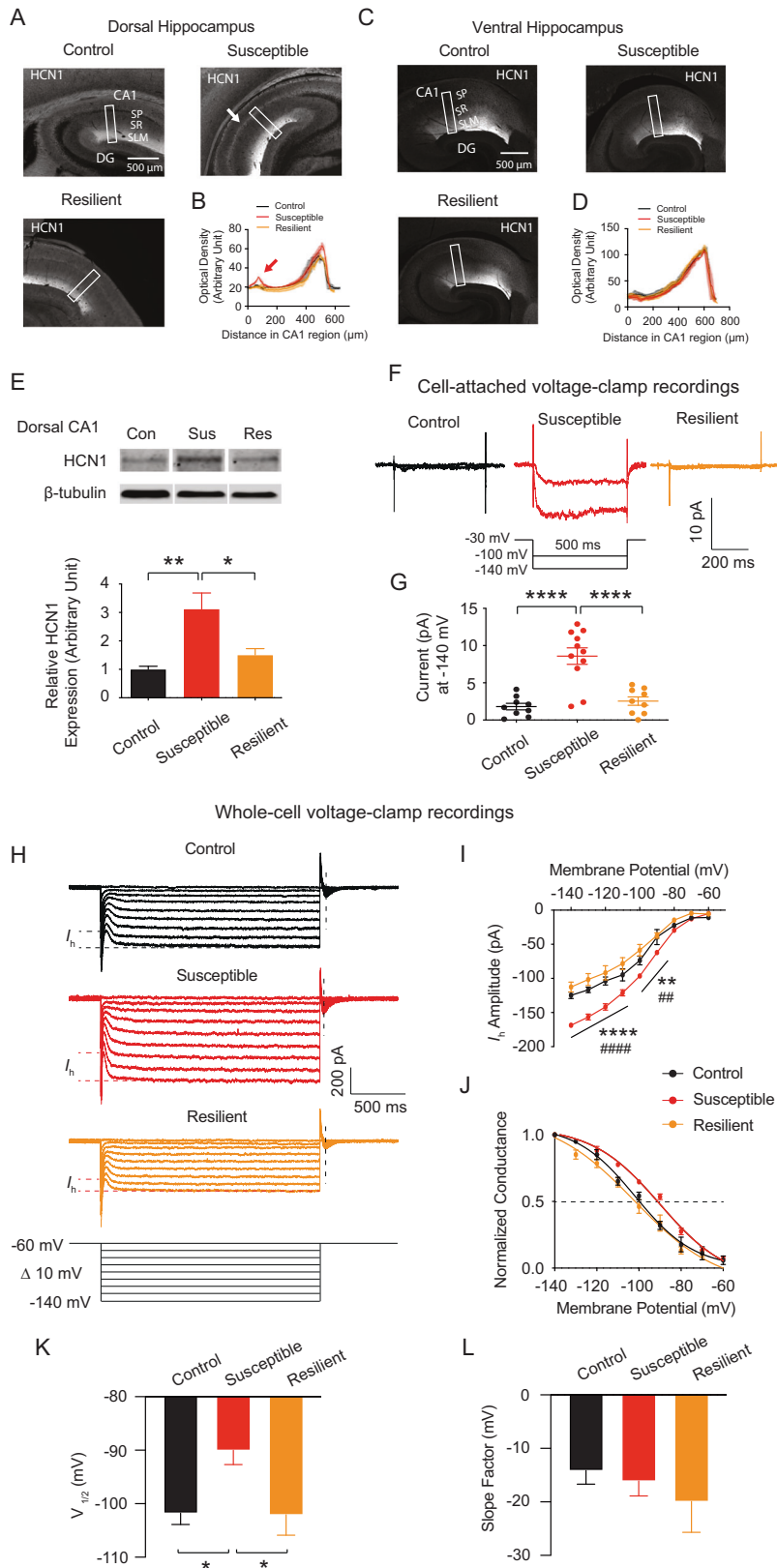
Corticosterone increased I_h as well as TRIP8b and HCN1 protein expression

At RMP, HCN channels are active, leading to a depolarized membrane potential and a decrease in R_{in} [38]. Furthermore, we observed the effects of corticosterone on dorsal CA1 neurons/region within 30 min, indicating that gene expression was not a factor. TRIP8b (also known as PEX5R) regulates HCN channel function and trafficking in the brain [64–66]. We investigated whether corticosterone-induced increased functional I_h (i.e., decreased R_{in}) in dorsal CA1 neurons was due to the increased HCN channel trafficking. We used a 50 μ m thick resection from either vehicle- or corticosterone-pretreated dorsal hippocampal

slices (300 μ m thick) for immunohistochemistry (Fig. 5A). Indeed, TRIP8b was significantly increased in the perisomatic CA1 region of dorsal hippocampus following corticosterone pretreatment (Fig. 5B, C). Consistent with this result, HCN1 protein expression was significantly increased in the perisomatic CA1 region of dorsal hippocampus (Fig. 5D, E). Furthermore, cell-attached recordings revealed that I_h was significantly increased in dorsal CA1 neurons (Fig. 5F, G), which was consistent with corticosterone-induced elevation of TRIP8b and HCN1 protein expression in the perisomatic CA1 region of dorsal hippocampus.

Corticosterone-induced upregulation of functional I_h was mediated by the GR, HCN channels, and the PKA but not the CamKII pathway

We next investigated whether the effects of corticosterone on functional I_h were via the GR activation. Dexamethasone is a selective GR agonist ($K_d = 4.6$ nM) [67, 68]. We examined if dexamethasone mimicked the effects of corticosterone. We employed 100 nM dexamethasone based on physiological responses in hippocampal CA1 neurons [69]. We tested if the lower concentration (25 nM) of dexamethasone had physiological



effects on CA1 neurons before using the 100 nM dexamethasone. RMP (Fig. S8A, B), R_{in} at RMP (Fig. S8A, C), and action potential firing at RMP (Fig. S8D, E) were unaffected by 25 nM dexamethasone, but 100 nM dexamethasone reduced R_{in} at RMP (Figs. 5H, I

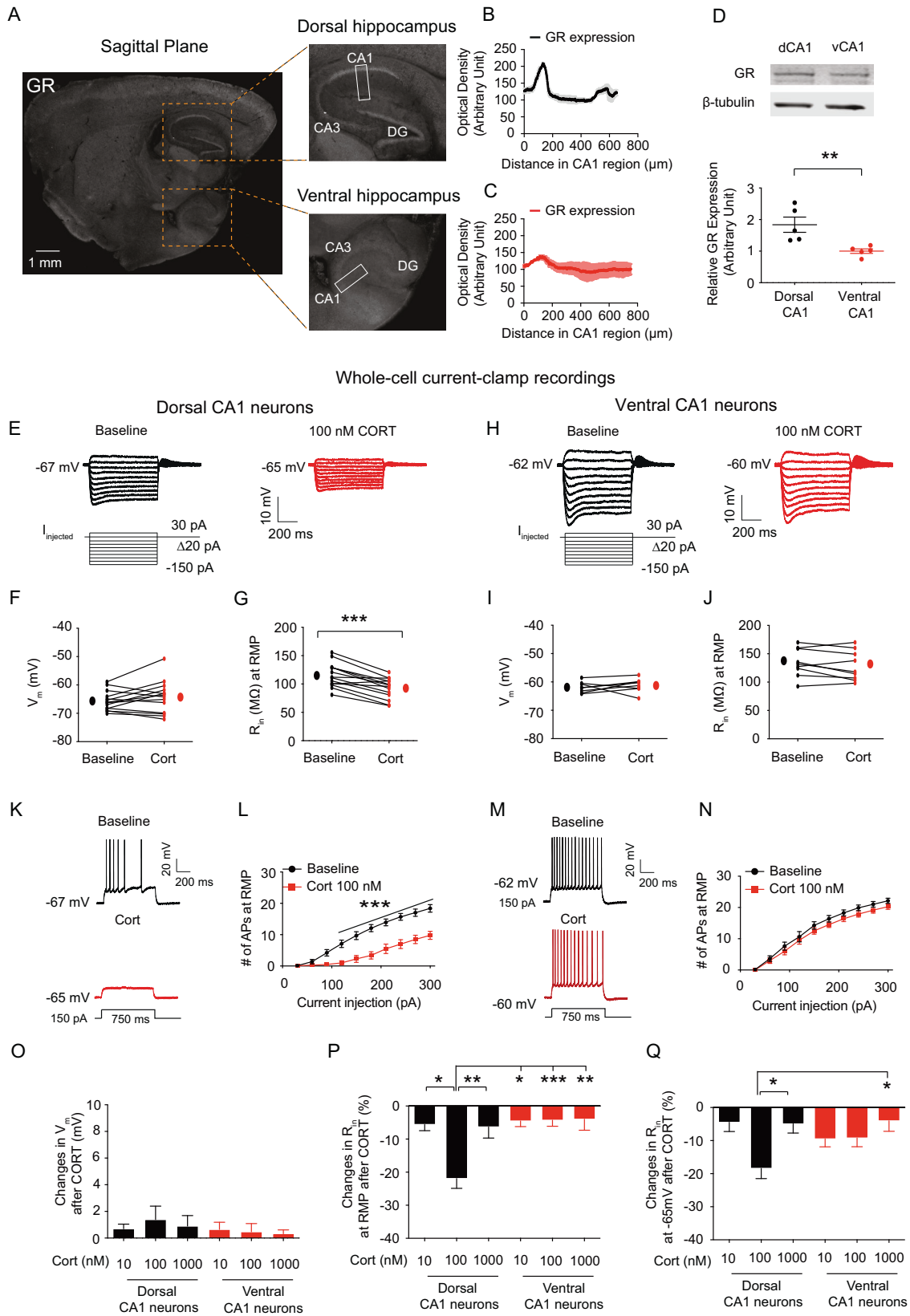
and S8F, H), R_{in} at -65 mV (Fig. 5J, K), and action potential firing at RMP (Fig. S8I, J) without affecting RMP (Fig. S8F, G). RU 486 (IC₅₀ = 2.6 nM) is a potent selective antagonist of GR receptors [70]. 500 nM RU 486 is sufficient to block corticosterone-mediated

Fig. 3 HCN1 protein expression and I_h were significantly increased in dorsal CA1 region/neurons from susceptible group. **A, C** Representative dorsal and ventral hippocampal slices immunolabeled with antibody against HCN1. Rectangle boxes depict the region of the slice used for quantification of the optical density. The arrows indicate increased perisomatic HCN1 protein expression. **B, D** Quantification of HCN1 protein expression from the perisomatic region to the distal dendritic region of CA1 from the dorsal and ventral hippocampi. **E** Western blot (top) and quantification (bottom) of HCN1 protein in dorsal CA1 region from the control, susceptible, and resilient groups. **F, G** We performed cell-attached voltage-clamp recordings. **F** Representative maximal h current traces in response to a 500-ms hyperpolarizing voltage step (-140 mV). **G** I_h was significantly increased in dorsal CA1 neurons from susceptible group compared with those from the control and resilient groups. **H–L** We performed whole-cell voltage-clamp recordings. **H** Representative current responses with step voltage commands ranging from -140 mV to -60 mV ($\Delta = 10$ mV) at a holding potential of -60 mV. The approximate position for determining the peak tail current is shown by black vertical dashed lines. **I** Susceptible group showed increased I_h in the dorsal CA1 neurons compared with those from the control and resilient groups. **J** The voltage dependence of activation for h channel was determined from tail currents ($I_h / I_{h, \max}$). The activation curve was fitted with a Boltzmann function with the following values: control $V_{1/2} = -101.8$ mV, $k = -14.13$ mV, susceptible $V_{1/2} = -90.02$ mV, $k = -16.09$ mV, resilient $V_{1/2} = -102.1$ mV, $k = -19.9$ mV. **K** The half-activation voltage of h channel ($V_{1/2}$) for susceptible group was significantly shifted to the right by around $+10$ mV, whereas **L** the slope factor was not different between groups. Data are expressed as mean \pm SEM.

physiological effects on hippocampal CA1 neurons [62]. We used RU 486 at a concentration of 500 nM. As a control experiment, 100 nM corticosterone lowered R_{in} at RMP (Fig. 5H, I), and at -65 mV (Fig. 5J, K). When dorsal CA1 neurons were pretreated with 500 nM RU 486, corticosterone had no effects on R_{in} at RMP (Figs. 5H, I and S9A–C), and at -65 mV (Fig. 5J, K). Furthermore, corticosterone-induced decreased neuronal excitability at RMP was blocked by GR antagonist RU 486 (Fig. S9D, E). These results indicate that corticosterone-induced changes in functional I_h were mediated by the activation of GR. The PKA pathway is involved in non-genomic glucocorticoid-GR effects [71, 72]. In addition, I_h maximal conductance is modulated by PKA-dependent phosphorylation [73]. We, therefore, investigated if the PKA pathway was required for the rapid corticosterone-induced changes in functional I_h . KT5720 ($K_i = 60$ nM) is a potent, selective inhibitor of PKA signaling [74]. As previously reported, we employed KT5720 at a concentration of 500 nM [63, 75]. In the presence of KT5720, we investigated the effects of corticosterone on functional I_h . R_{in} at RMP (Figs. 5H, I and S10A–C), R_{in} at -65 mV (Fig. 5J, K), and the number of action potentials at RMP (Fig. S10D, E) were unaffected following corticosterone treatment in dorsal CA1 neurons, suggesting that corticosterone-mediated effects on functional I_h were dependent on the PKA pathway. Given that 100 nM corticosterone enhanced calcium current amplitude via the GR activation [61], we next investigated whether the CamKII was required for the effects on functional I_h in dorsal CA1 neurons. KN-62 is a selective inhibitor of CamKII with k_i of $0.9 \mu\text{M}$ [76]. $5 \mu\text{M}$ KN-62 blocks the CamKII pathway, as previously described [63, 77]. We, therefore, used KN-62 at a concentration of $5 \mu\text{M}$. Despite KN-62 blocking the CamKII signaling pathway, we observed changes in R_{in} at RMP (Fig. 5H, I and S11A–C), R_{in} at -65 mV (Fig. 5J, K), and the number of action potentials at RMP (Fig. S11D, E) following corticosterone treatment in dorsal CA1 neurons. These results imply that corticosterone-mediated changes in functional I_h was not mediated by the CamKII pathway. We next examined if corticosterone-induced changes in functional I_h were mediated directly by HCN channels. ZD7288 is a potent HCN channel blocker at a concentration range of 10 to $20 \mu\text{M}$ [34, 44]. The effects of corticosterone in dorsal CA1 neurons were determined in the presence of the ZD7288. In a previous study, we observed that using ZD7288 in the bath caused nonspecific effects, such as progressive depolarization 10–15 min after the hyperpolarization of V_m [34]. To circumvent this, we used ZD7288 in the pipette ($20 \mu\text{M}$) instead of the bath application. As predicted from a blockage of HCN channels, ZD7288 caused a significant hyperpolarization of the RMP (Fig. S12A), increased R_{in} at RMP (Fig. S12B) and at -65 mV (Fig. S12C) compared to control group. When HCN channels were blocked, the corticosterone had no effects on RMP (Fig. S12D, E), R_{in} at RMP (Figs. 5H, I and S12D, F), R_{in} at -65 mV (Fig. 5J, K), and the number of action potentials at -65 mV (Fig. S12G, H).

Susceptible mice displayed a persistent social avoidance, which was linked to increased I_h and were insensitive to corticosterone effects

One of the most distressing symptoms of PTSD is the recurrence of the experience [1]. A longitudinal study of PTSD patients reveals that they have PTSD symptoms even 50 or more years after their traumatic experience [78, 79]. In CSDS paradigm, naive mice were repeatedly exposed to aggressor mice. After 12 days in this physically and emotionally stressful environment, naive mice showed susceptible (i.e., increased social avoidance) and resilient (i.e., normal-like social interaction) phenotypes during the social interaction test. These susceptible mice had a painful recollection of aggressor mice. Furthermore, these impaired behavioral results were linked to (1) decreased neuronal excitability, (2) increased perisomatic HCN1 protein expression, and (3) elevated I_h in dorsal but not ventral CA1 region/neurons. We, first, examined if susceptible mice exposed to novel aggressor mice re-experienced the trauma during the social interaction test. Because the difference in human age between mice aged 3 months and 6 months is over 10 years [80], we chose re-exposure periods of 1 month and 3 months with singly housed 3-month-old CSDS-treated and control mice. As a result, we can see whether (1) CSDS-induced social avoidance lasted for a long period and (2) social avoidance was linked to pathological changes in I_h . CSDS was subjected to male mice aged 6 to 7 weeks for 12 days (Fig. 6A). During the social interaction test, CSDS produced susceptible and resilient phenotypes (Figs. 6B and S13A). Susceptible mice demonstrated re-experiencing trauma such as social avoidance after one month (Figs. 6C and S13A) and three months (Figs. 6D and S13A) without CSDS. Because dorsal CA1 neurons from susceptible mice had lower neuronal excitability than the control and resilient mice, we investigated the physiological effects on dorsal CA1 neurons following behavioral tests after 3 months without CSDS. Acute dorsal hippocampal slices were prepared after behavioral tests [43]. After acute hippocampal slicing, we set aside tissue samples for immunohistochemistry. Electrophysiological data and protein expression might therefore be connected. Dorsal CA1 neurons from susceptible group displayed lower neuronal excitability than the control and resilient groups (Fig. 6E, F), which was consistent with earlier findings (Fig. 2D, E). Interestingly, resilient group showed higher neuronal excitability of dorsal CA1 neurons than that of the control and susceptible groups (Fig. 6E, F). In comparison to the control and resilient groups, cell-attached patch-clamp recordings indicated a substantial increase in I_h in dorsal CA1 neurons from susceptible group (Fig. 6G, H). We next investigated whether HCN1 and TRIP8b protein expression were changed along the somatodendritic axis of dorsal CA1 neurons. HCN1 (Fig. 6I, J) and TRIP8b (Fig. 6K, L) protein expression in susceptible group were considerably increased in the perisomatic CA1 region of the dorsal hippocampus, consistent with increased I_h . Corticosterone



increased TRIP8b and HCN1 protein expression in vitro hippocampus slices, leading to an increase in I_h through GRs and HCN channels (Fig. 5). We next investigated whether corticosterone-induced changes in functional I_h (i.e., R_{in}) were altered between

groups. RMP was unaffected by corticosterone in any of the groups (Fig. S14A, B). Before treating corticosterone, dorsal CA1 neurons from susceptible group had lower R_{in} at RMP (Fig. 6M) and at -65 mV (Fig. S14C) than the control and resilient group,

Fig. 4 Dorsal CA1 neurons responded to corticosterone more strongly than ventral CA1 neurons. **A** Representative sagittal section of brain showing GR immunoreactivity in dorsal (top) and ventral (bottom) hippocampi. Rectangle boxes depict the region of the slice used for quantification of optical density. **B, C** Quantification of GR protein expression from the perisomatic region to the distal dendritic region of CA1 from the dorsal and ventral hippocampi. **D** Western blot (top) and quantification (bottom) of GR protein in CA1 region from the dorsal and ventral hippocampi. **E–Q** We performed whole-cell current-clamp recordings. **E, H** Representative voltage responses with step current commands ranging from -150 pA to $+30$ pA ($\Delta = 20$ pA) at RMP before and after bath application of corticosterone. Corticosterone lowered R_{in} (**G**) but had no impact on RMP (**F**) in dorsal CA1 neurons. There are no changes in RMP (**I**) and R_{in} (**J**) in ventral CA1 neurons following corticosterone treatment. Representative voltage responses with depolarizing current step (150 pA; 750 ms) at RMP in dorsal (**K**) and ventral (**M**) CA1 neurons. **L** Dorsal CA1 neurons had decreased action potential firing at RMP following corticosterone treatment. **N** Action potential firing at RMP was not altered in ventral CA1 neurons following corticosterone treatment. **O** Corticosterone doses of 10 nM, 100 nM, and 1 μ M had no effect on RMP of CA1 neurons in dorsal and ventral hippocampi. 100 nM corticosterone significantly reduced R_{in} at RMP (**P**) and at -65 mV (**Q**) in dorsal CA1 neurons compared to 10 nM and 1 μ M corticosterone. When compared to 10 nM and 1 μ M corticosterone, 100 nM corticosterone had no impact on R_{in} at RMP (**P**) and at -65 mV (**Q**) in ventral CA1 neurons. Data are expressed as mean \pm SEM.

consistent with elevated I_h . When dorsal CA1 neurons were treated with corticosterone, control and resilient groups displayed reduced R_{in} at RMP (Fig. 6M, N) and at -65 mV (Fig. S14C, D). Surprisingly, corticosterone had no additional effect on R_{in} at RMP (Fig. 6M, N) and at -65 mV (Fig. S14C, D) in dorsal CA1 neurons from susceptible group.

DISCUSSION

We found that social avoidance and impaired spatial working memory were seen in susceptible mice, which were linked to increased perisomatic HCN1 protein expression, higher I_h , and lower neuronal excitability in the dorsal but not ventral CA1 neurons. In control mice, bath application of corticosterone had effects similar to those in susceptible mice. Corticosterone in the bath reduced R_{in} , lowered neuronal excitability, increased TRIP8b and HCN1 protein expression, and elevated I_h in the dorsal but not ventral CA1 region/neurons. These corticosterone-induced alterations in functional I_h depended on the GR, HCN channels, and the PKA but not the CamKII pathway. Finally, susceptible mice re-exposed to new aggressor mice after one month or three months without CSDS displayed social avoidance. This persistent behavioral deficit in susceptible mice was associated with increased perisomatic TRIP8b and HCN1 protein expression, elevated I_h , reduced R_{in} , and lower neuronal excitability in the dorsal CA1 region/neurons. Furthermore, alterations in functional I_h caused by corticosterone-GR activation were not observed in the dorsal CA1 neurons of susceptible mice but were seen in control and resilient mice.

PTSD is a severe mental condition that can develop due to life-threatening events. One of the most common PTSD symptoms is avoidance. Experiential avoidance is the key to making a traumatized person more likely to develop and maintain PTSD [11]. CSDS is a rodent model of psychosocial stress that causes social avoidance and anhedonia [14], indicators of human PTSD. Interestingly, some repeatedly socially defeated mice have susceptible phenotypes, while others do not [14], similar to human PTSD. Although women are twice as likely as men to suffer from PTSD [81], using the CSDS paradigm with female mice/rats is complicated and unreliable [82]. We attempted to use female mice in CSDS. However, ovariectomized female CD-1 mice had a considerably lower frequency of physical attack, a shorter attack duration, and a longer attack latency than male aggressor CD-1 mice (Data not shown). Unlike the female mice in CSDS, chronic socially defeated male mice exhibited anxiogenic-like behavior in the elevated plus-maze test. During the social interaction test, some defeated male mice had a traumatic memory of aggressor male mice, which caused them to avoid social engagement (i.e., social avoidance). The social avoidance persisted for at least three months when susceptible male mice were reintroduced to new aggressor male mice. Furthermore, in the Y maze test, susceptible male mice had worse spatial working memory. Overall, our animal model produced behavioral deficits in some populations of

traumatic event-exposed male mice, comparable to those seen in human PTSD.

We initially examined the neuronal excitability of dorsal and ventral CA1 neurons in control, susceptible, and resilient male mice since hippocampal hypoactivity has been linked to human PTSD [83]. After 12 days of CSDS, susceptible mice had decreased R_{in} and lower neuronal excitability in the dorsal but not ventral CA1 neurons compared to control and resilient groups. In addition, dorsal CA1 neurons of the susceptible group showed increased HCN1 protein expression and elevated I_h . HCN channels are partially active at the resting membrane potential, producing a non-inactivating, depolarizing inward current. Given that its reversal potential is around -30 mV, I_h should exert an excitatory action by depolarizing the membrane potential toward the action potential threshold. However, HCN1 channels are highly enriched in distal dendrites of the hippocampal CA1 region, providing a paradoxical inhibitory action such as reduction of synaptic integration and decreased neuronal excitability by input resistance [38]. This paradoxical inhibitory effect of I_h might depend on the interaction with other ionic conductances (e.g., delayed-rectifier M-type K^+ channels) in hippocampal and cortical pyramidal neurons [84]. Surprisingly, after three months without CSDS, dorsal CA1 neurons from susceptible mice had lower R_{in} and neuronal excitability. However dorsal CA1 neurons from resilient mice had higher R_{in} and neuronal excitability than control and susceptible groups (Fig. 6). Compared to the results from Figs. 1 and 2 (i.e., no cessation of CSDS), hypo-neuronal excitability of dorsal CA1 neurons was persistent in susceptible mice. In contrast, resilient mice had hyper-neuronal excitability of dorsal CA1 neurons. Further research is needed to understand how mice exposed to traumatic events develop resilient phenotypes associated with increased R_{in} and neuronal excitability. Regardless of this, neuronal excitability of dorsal CA1 neurons might be the cellular mechanism underpinning the development of susceptibility and resilience to social avoidance. Consistent with our findings, mice infused with corticosterone in the dorsal CA1 region produce PTSD-like memories such as emotional hypermnnesia and contextual amnesia [85–87]. Normal mice display PTSD-like memory when dorsal CA1 neurons are inhibited by optogenetic inhibition during stress. On the other hand, optogenetic activation of dorsal CA1 neurons during stress prevents PTSD-like memory [85]. It has been reported that the dorsal hippocampus has more GR protein expression than the ventral hippocampus [88, 89]. Consistent with these reports, we also found that GR protein expression was more significant in the dorsal hippocampus than in the ventral hippocampus. Interestingly, GR protein was highly concentrated in the dorsal CA1 perisomatic area but not in the ventral CA1 region (Fig. 4). In our previous studies, blocking the SERCA pumps in dorsal CA1 neurons, which elevate intracellular calcium levels, increases I_h and functional I_h (i.e., reduced R_{in} and lower neuronal excitability) [43, 63]. Corticosterone-GR activation has been shown to enhance Ca^{2+} current amplitude in rat/mouse hippocampal CA1 neurons [61, 62]. Indeed, dorsal CA1 neurons

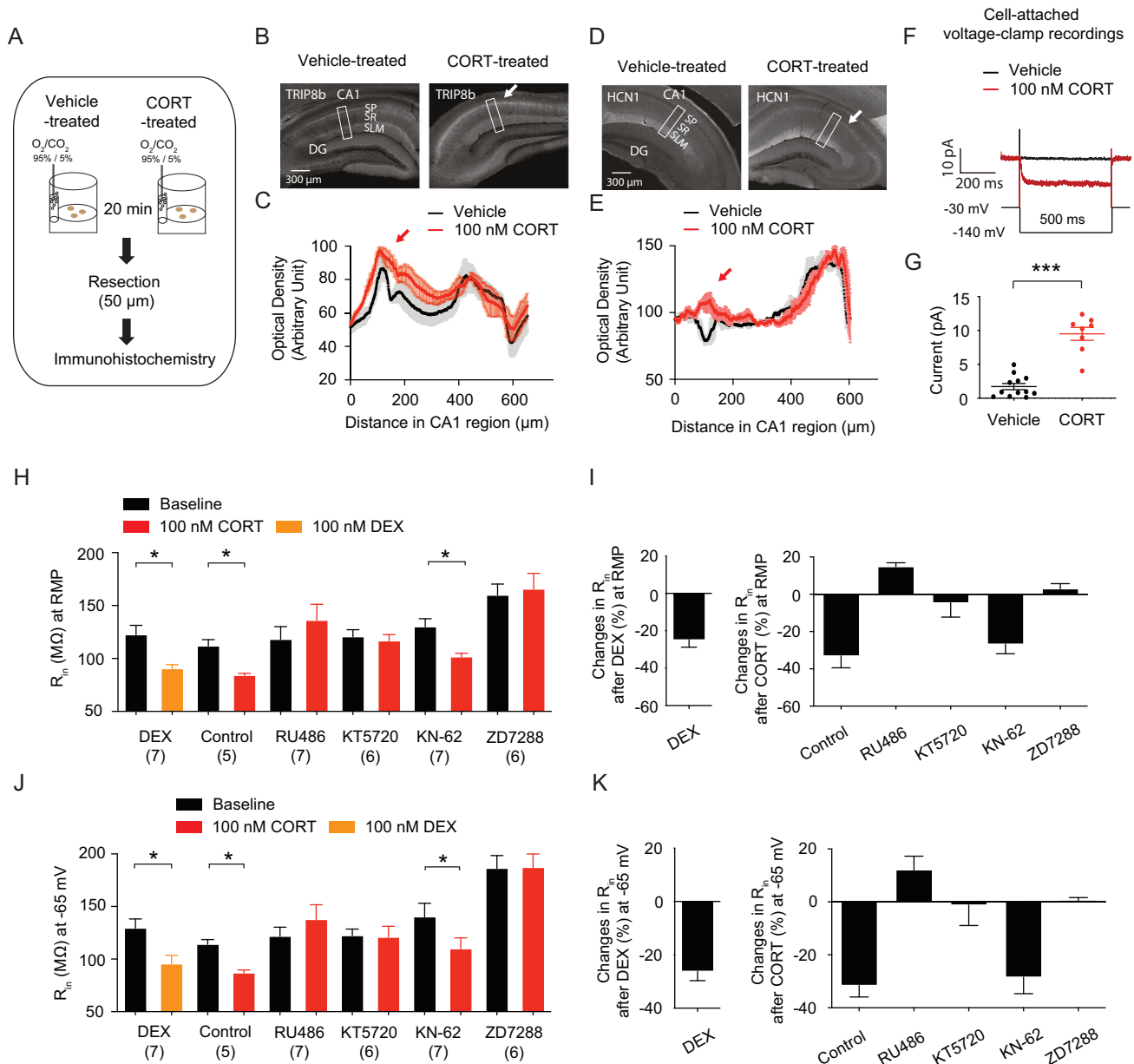
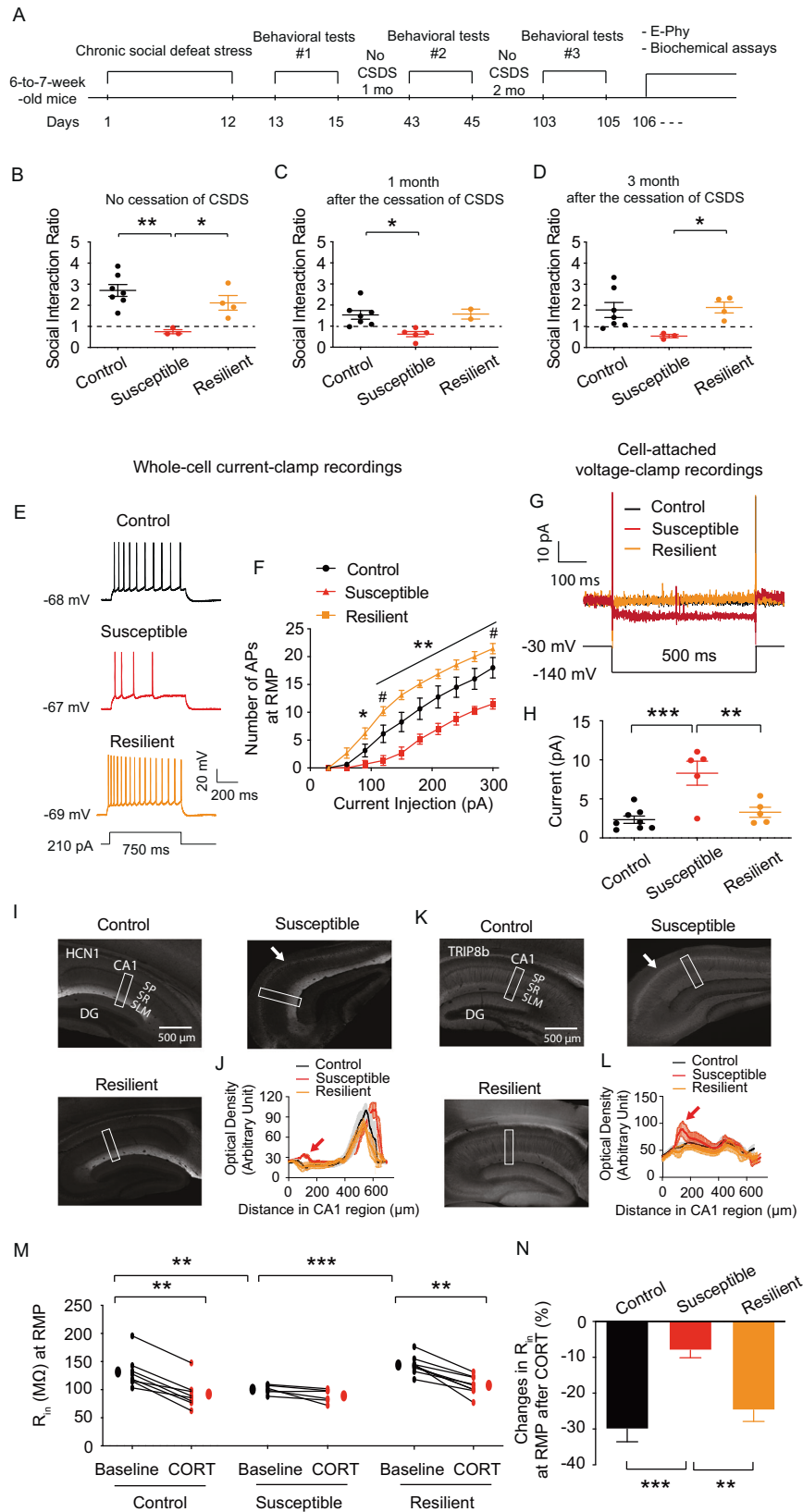


Fig. 5 The GR, HCN channels, and the PKA pathway were all involved in corticosterone-induced upregulation of functional *I_h*. **A** Illustration depicting the acute corticosterone treatment in the dorsal hippocampus. **B** Representative dorsal hippocampal slices immunolabeled with antibody against TRIP8b. Rectangle boxes depict the region of the slice used for quantification of the optical density. The arrows indicate increased perisomatic TRIP8b protein expression. **C** Quantification of TRIP8b protein expression from the perisomatic region to the distal dendritic region of CA1 from the dorsal hippocampus. **D** Representative dorsal hippocampal slices immunolabeled with antibody against HCN1. Rectangle boxes depict the region of the slice used for quantification of the optical density. The arrows indicate increased perisomatic HCN1 protein expression. **E** Quantification of HCN1 protein expression from the perisomatic region to the distal dendritic region of CA1 from the dorsal hippocampus. **F, G** We performed cell-attached voltage-clamp recordings. **F** Representative maximal *h* current traces in response to a 500-ms hyperpolarizing voltage step (-140 mV). **G** *I_h* was significantly elevated in the dorsal CA1 neurons from corticosterone treatment compared with those from the vehicle-treated group. Dexamethasone reduced *R_{in}* at RMP (**H**) and at -65 mV (**J**) in dorsal CA1 neurons. Corticosterone-induced decrease in *R_{in}* at RMP (**H**) and at -65 mV (**J**) was blocked by RU 486, KT5720, and ZD7288. Changes in *R_{in}* at RMP (**I**) and at -65 mV (**K**) were blocked by RU 486, KT5720, and ZD7288. Data are expressed as mean ± SEM.

had decreased *R_{in}* and lower neuronal excitability following corticosterone treatment (Fig. 4). Dexamethasone, a selective GR agonist, elicited physiological responses in dorsal CA1 neurons similar to those of corticosterone. When dorsal CA1 neurons were pretreated with GR antagonist (RU 486), the effects of corticosterone on *R_{in}* and neuronal excitability were blocked (Fig. 5). Furthermore, decreased *R_{in}* and neuronal excitability caused by corticosterone treatment were blocked by the HCN channel blocker (ZD7288) (Fig. 5). These findings indicate that

corticosterone reduced *R_{in}* and neuronal excitability through activating GR and HCN channels. HCN1 protein is abundant in the CA1 area of the hippocampus, with a gradient of increasing channel density from the soma to the distal apical dendrites [38, 39]. The aberrant HCN1 protein subcellular distribution along the somatodendritic axis of CA1 neurons is linked to pathogenic events in the animal models of depression and temporal lobe epilepsy [43, 44, 90]. Because corticosterone reduced *R_{in}* and neuronal excitability of dorsal CA1 neurons from control mice,



we looked to see if corticosterone affected the protein expression of HCN1 and TRIP8b, the primary auxiliary subunit of HCN channels. Pretreatment with corticosterone for 20–30 min increased perisomatic TRIP8b protein expression, which led to

higher perisomatic HCN1 protein expression. Cell-attached recordings and whole-cell voltage-clamp recordings showed that corticosterone increased I_h in the dorsal CA1 neurons. PKA-dependent phosphorylation is involved in the control of I_h

Fig. 6 Susceptible mice re-exposed to novel aggressor mice displayed a persistent social avoidance, which was associated with elevated I_h and was insensitive to corticosterone effects. **A** Timeline of CSDS, behavioral tests, electrophysiology, and biochemical assay. **B** CSDS produced the susceptible and resilient phenotype during the social interaction test. After 1 month (**C**) or 3 months (**D**) of no CSDS, susceptible mice showed persistent social avoidance during the social interaction test. **E, F** We performed whole-cell current-clamp recordings. **E** Representative voltage responses with depolarizing current step (210 pA; 750 ms) at RMP in dorsal CA1 neurons. **F** Dorsal CA1 neurons of susceptible group had lower action potential firing than control group, whereas the resilient group had higher action potential firing. **G, H** We performed cell-attached voltage-clamp recordings. **G** Representative maximal h current traces in response to a 500-ms hyperpolarizing voltage step (-140 mV). **H** I_h was significantly elevated in the dorsal CA1 neurons from susceptible group compared with those from the control and resilient mice. Representative dorsal hippocampal slices immunolabeled with antibody against HCN1 (**I**) and TRIP8b (**K**). Rectangle boxes depict the region of the slice used for quantification of the optical density. The arrows indicate increased perisomatic HCN1 and TRIP8b protein expression. Quantification of HCN1 (**J**) and TRIP8b (**L**) protein expression from the perisomatic region to the distal dendritic region of CA1 from the dorsal hippocampus. **M, N** We performed whole-cell current-clamp recordings. **M** Corticosterone reduced R_{in} at RMP of the dorsal CA1 neurons in the control and resilient groups, but had no effect on R_{in} in susceptible group. **N** Changes in R_{in} at RMP were much lower in susceptible group compared to the control and resilient groups. Data are expressed as mean \pm SEM.

maximal conductance [73]. When dorsal CA1 neurons were pretreated with the PKA inhibitor (KT5720), the effects of corticosterone on functional I_h were blocked (Fig. 5). As a result, rapid effects of corticosterone on functional I_h were mediated by the expression of TRIP8b and HCN1 protein and the PKA pathway. When dorsal CA1 neurons from control mice were treated with corticosterone, R_{in} and neuronal excitability were both decreased, which was similar to the results from susceptible mice. Furthermore, dorsal CA1 neurons from the susceptible mice had no further changes in functional I_h (i.e., R_{in}) following corticosterone treatment, whereas control and resilient mice did. These findings imply that elevated I_h in the dorsal CA1 neurons from susceptible mice occluded corticosterone-induced upregulation of functional I_h .

Selective serotonin reuptake inhibitors are Food and Drug Administration-approved medications for treating PTSD that primarily act by targeting the monoamine system and raising serotonin levels in limbic brain regions, such as the hippocampus. However, after the initial pharmacologic treatment, only around 20–30% of patients with PTSD satisfy remission criteria [91, 92]. Despite its significant side effects, such as psychotomimetic symptoms and the danger of drug abuse, (R,S)-ketamine has an immediate therapeutic impact on human PTSD [93, 94]. (S)-ketamine is an HCN1 inhibitor [44, 95] and an antagonist of the N-methyl-D-aspartate receptor [96]. Pretreatment with (S)-ketamine before the beginning of CUS prevented aberrant behaviors (i.e., anxiogenic- and depressive-like behaviors) and neuropathological alterations caused by CUS (i.e., upregulation of perisomatic I_h and a decrease in neuronal excitability) [43, 44]. A reduction of HCN1 protein expression in the dorsal CA1 region (about 30% of the dorsal CA1 region) before the CUS-induced onset of depression and anxiety is sufficient to provide resilient effects to CUS [43]. Corticosterone-GR activation-induced lower neuronal excitability was blocked by the HCN channel blocker (Fig. 6). This finding might explain why knockdown of HCN1 protein expression or pretreatment of (S)-ketamine before the onset of depression and anxiety provides resilient effects [43, 44].

In conclusion, we have demonstrated that susceptible mice displayed social avoidance and impaired spatial working memory. In dorsal CA1 neurons, susceptible mice reduced neuronal excitability, whereas resilient mice had increased neuronal excitability. These results suggest that the neuronal excitability of dorsal CA1 neurons might be the cellular mechanism underlying the development of susceptibility and resilience to social avoidance. Acute corticosterone treatment in dorsal CA1 neurons from control mice, where perisomatic GR was strongly expressed, produced comparable effects, as seen by susceptible mice. These effects of corticosterone were mediated by the GR, HCN channels, and the PKA pathway. Importantly, corticosterone did not affect functional I_h in dorsal CA1 neurons from susceptible mice, while it affected the control and resilient groups. Our findings imply that abnormal subcellular expression of HCN1 protein along the somatodendritic axis of dorsal CA1 neurons contributes to a

reduction in neuronal excitability and may be the molecular mechanism underpinning the development of susceptibility to social avoidance.

REFERENCES

- American_Psychiatric_Association. Diagnostic and Statistical Manual of Mental Disorders 5th Edn. Washington, DC: American Psychiatric Association; 2013.
- Kessler RC. Posttraumatic stress disorder: the burden to the individual and to society. *J Clin Psychiatry*. 2000;61:4–12.
- Buckley TC, Mozley SL, Bedard MA, Dewulf AC, Greif J. Preventive health behaviors, health-risk behaviors, physical morbidity, and health-related role functioning impairment in veterans with post-traumatic stress disorder. *Mil Med*. 2004;169:536–40.
- Haviland MG, Banta JE, Sonne JL, Przekop P. Posttraumatic Stress Disorder-Related Hospitalizations in the United States (2002–11): Rates, Co-Occurring Illnesses, Suicidal Ideation/Self-Harm, and Hospital Charges. *J Nerv Ment Dis*. 2016;204:78–86.
- Rytwinski NK, Scur MD, Feeny NC, Youngstrom EA. The co-occurrence of major depressive disorder among individuals with posttraumatic stress disorder: a meta-analysis. *J Trauma Stress*. 2013;26:299–309.
- Wilder Schaaf KP, Artman LK, Peberdy MA, Walker WC, Ornato JP, Gossip MR, et al. Anxiety, depression, and PTSD following cardiac arrest: a systematic review of the literature. *Resuscitation*. 2013;84:873–7.
- Bernal M, Haro JM, Bernert S, Brugha T, de Graaf R, Bruffaerts R, et al. Risk factors for suicidality in Europe: results from the ESEMED study. *J Affect Disord*. 2007;101:27–34.
- Cogle JR, Keough ME, Riccardi CJ, Sachs-Ericsson N. Anxiety disorders and suicidality in the National Comorbidity Survey-Replication. *J Psychiatr Res*. 2009;43:825–9.
- Hayes SC, Wilson KG, Gifford EV, Follette VM, Strosahl K. Experimental avoidance and behavioral disorders: a functional dimensional approach to diagnosis and treatment. *J Consult Clin Psychol*. 1996;64:1152–68.
- Polusny MA, Rosenthal MZ, Aban I, Follette VM. Experimental avoidance as a mediator of the effects of adolescent sexual victimization on negative adult outcomes. *Violence Vict*. 2004;19:109–20.
- Leonard KA, Ellis RA, Orcutt HK. Experiential avoidance as a mediator in the relationship between shame and posttraumatic stress disorder: The effect of gender. *Psychol Trauma*. 2020;12:651–8.
- Kashdan TB, Morina N, Priebe S. Post-traumatic stress disorder, social anxiety disorder, and depression in survivors of the Kosovo War: experiential avoidance as a contributor to distress and quality of life. *J Anxiety Disord*. 2009;23:185–96.
- Thompson BL, Waltz J. Mindfulness and experiential avoidance as predictors of posttraumatic stress disorder avoidance symptom severity. *J Anxiety Disord*. 2010;24:409–15.
- Krishnan V, Han MH, Graham DL, Berton O, Renthal W, Russo SJ, et al. Molecular adaptations underlying susceptibility and resistance to social defeat in brain reward regions. *Cell*. 2007;131:391–404.
- Wang Z, Neylan TC, Mueller SG, Lenoci M, Truran D, Marmor CR, et al. Magnetic resonance imaging of hippocampal subfields in posttraumatic stress disorder. *Arch Gen Psychiatry*. 2010;67:296–303.
- Morey RA, Haswell CC, Hooper SR, De Bellis MD. Amygdala, Hippocampus, and Ventral Medial Prefrontal Cortex Volumes Differ in Maltreated Youth with and without Chronic Posttraumatic Stress Disorder. *Neuropsychopharmacology*. 2016;41:791–801.
- Pitman RK, Shin LM, Rauch SL. Investigating the pathogenesis of posttraumatic stress disorder with neuroimaging. *J Clin Psychiatry*. 2001;62:47–54.

18. Bremner JD, Vermetten E, Afzal N, Vythilingam M. Deficits in verbal declarative memory function in women with childhood sexual abuse-related posttraumatic stress disorder. *J Nerv Ment Dis.* 2004;192:643–9.
19. Shin LM, Shin PS, Heckers S, Krangel TS, Macklin ML, Orr SP, et al. Hippocampal function in posttraumatic stress disorder. *Hippocampus.* 2004;14:292–300.
20. Speer KE, Semple S, Naumovski N, D'Cunha NM, McKune AJ. HPA axis function and diurnal cortisol in post-traumatic stress disorder: A systematic review. *Neurobiol Stress.* 2019;11:100180.
21. Yehuda R, Keefe RS, Harvey PD, Levengood RA, Gerber DK, Geni J, et al. Learning and memory in combat veterans with posttraumatic stress disorder. *Am J Psychiatry.* 1995;152:137–9.
22. Jacobson L, Sapolsky R. The role of the hippocampus in feedback regulation of the hypothalamic-pituitary-adrenocortical axis. *Endocr Rev.* 1991;12:118–34.
23. Elzinga BM, Schmahl CG, Vermetten E, van Dyck R, Bremner JD. Higher cortisol levels following exposure to traumatic reminders in abuse-related PTSD. *Neuropsychopharmacology.* 2003;28:1656–65.
24. Heim C, Newport DJ, Heit S, Graham YP, Wilcox M, Bonsall R, et al. Pituitary-adrenal and autonomic responses to stress in women after sexual and physical abuse in childhood. *JAMA.* 2000;284:592–7.
25. Liberzon I, Abelson JL, Flagel SB, Raz J, Young EA. Neuroendocrine and psychophysiological responses in PTSD: a symptom provocation study. *Neuropsychopharmacology.* 1999;21:40–50.
26. Newcomer JW, Selke G, Melson AK, Hershey T, Craft S, Richards K, et al. Decreased memory performance in healthy humans induced by stress-level cortisol treatment. *Arch Gen Psychiatry.* 1999;56:527–33.
27. Keenan PA, Jacobson MW, Soleymani RM, Newcomer JW. Commonly used therapeutic doses of glucocorticoids impair explicit memory. *Ann N Y Acad Sci.* 1995;761:400–2.
28. Conrad CD, Galea LA, Kuroda Y, McEwen BS. Chronic stress impairs rat spatial memory on the Y maze, and this effect is blocked by tianeptine pretreatment. *Behav Neurosci.* 1996;110:1321–34.
29. Luine V, Villegas M, Martinez C, McEwen BS. Repeated stress causes reversible impairments of spatial memory performance. *Brain Res.* 1994;639:167–70.
30. Fanselow MS, Dong HW. Are the dorsal and ventral hippocampus functionally distinct structures? *Neuron.* 2010;65:7–19.
31. Moser MB, Moser EI. Functional differentiation in the hippocampus. *Hippocampus.* 1998;8:608–19.
32. Bannerman DM, Rawlins JN, McHugh SB, Deacon RM, Yee BK, Bast T, et al. Regional dissociations within the hippocampus-memory and anxiety. *Neurosci Biobehav Rev.* 2004;28:273–83.
33. Maren S, Holt WG. Hippocampus and Pavlovian fear conditioning in rats: muscimol infusions into the ventral, but not dorsal, hippocampus impair the acquisition of conditional freezing to an auditory conditional stimulus. *Behav Neurosci.* 2004;118:97–110.
34. Kim CS, Johnston D. A1 adenosine receptor-mediated GIRK channels contribute to the resting conductance of CA1 neurons in the dorsal hippocampus. *J Neurophysiol.* 2015;113:2511–23.
35. Pape HC. Queer current and pacemaker: the hyperpolarization-activated cation current in neurons. *Annu Rev Physiol.* 1996;58:299–327.
36. Brewster AL, Chen Y, Bender RA, Yeh A, Shigemoto R, Baram TZ. Quantitative analysis and subcellular distribution of mRNA and protein expression of the hyperpolarization-activated cyclic nucleotide-gated channels throughout development in rat hippocampus. *Cereb Cortex.* 2007;17:702–12.
37. Monteggia LM, Eisch AJ, Tang MD, Kaczmarek LK, Nestler EJ. Cloning and localization of the hyperpolarization-activated cyclic nucleotide-gated channel family in rat brain. *Brain Res Mol Brain Res.* 2000;81:129–39.
38. Magee JC. Dendritic hyperpolarization-activated currents modify the integrative properties of hippocampal CA1 pyramidal neurons. *J Neurosci: Off J Soc Neurosci.* 1998;18:7613–24.
39. Lorincz A, Notomi T, Tamas G, Shigemoto R, Nusser Z. Polarized and compartment-dependent distribution of HCN1 in pyramidal cell dendrites. *Nat Neurosci.* 2002;5:1185–93.
40. Biel M, Wahl-Schott C, Michalakis S, Zong X. Hyperpolarization-activated cation channels: from genes to function. *Physiol Rev.* 2009;89:847–85.
41. Lewis AS, Vaidya SP, Blais CA, Liu Z, Stoub TR, Brager DH, et al. Deletion of the Hyperpolarization-Activated Cyclic Nucleotide-Gated Channel Auxiliary Subunit TRIP8b Impairs Hippocampal Ih Localization and Function and Promotes Anti-depressant Behavior in Mice. *J Neurosci: Off J Soc Neurosci.* 2011;31:7424–40.
42. Kim CS, Chang PY, Johnston D. Enhancement of dorsal hippocampal activity by knockdown of HCN1 channels leads to anxiolytic- and antidepressant-like behaviors. *Neuron.* 2012;75:503–16.
43. Kim CS, Brager DH, Johnston D. Perisomatic changes in h-channels regulate depressive behaviors following chronic unpredictable stress. *Mol Psychiatry.* 2018;23:892–903.
44. Kim CS, Johnston D. Antidepressant Effects of (S)-Ketamine through a Reduction of Hyperpolarization-Activated Current Ih. *iScience.* 2020;23:101239.
45. Cao JL, Covington HE 3rd, Friedman AK, Wilkinson MB, Walsh JJ, Cooper DC, et al. Mesolimbic dopamine neurons in the brain reward circuit mediate susceptibility to social defeat and antidepressant action. *J Neurosci: Off J Soc Neurosci.* 2010;30:16453–8.
46. Zhong P, Vickstrom CR, Liu X, Hu Y, Yu L, Yu HG, et al. HCN2 channels in the ventral tegmental area regulate behavioral responses to chronic stress. *Elife.* 2018;7:e32420.
47. Golden SA, Covington HE 3rd, Berton O, Russo SJ. A standardized protocol for repeated social defeat stress in mice. *Nat Protoc.* 2011;6:1183–91.
48. Stuart GJ, Dodt HU, Sakmann B. Patch-clamp recordings from the soma and dendrites of neurons in brain slices using infrared video microscopy. *Pflug Arch.* 1993;423:511–8.
49. File SE, Seth P. A review of 25 years of the social interaction test. *Eur J Pharm.* 2003;463:35–53.
50. Pellow S, Chopin P, File SE, Briley M. Validation of open:closed arm entries in an elevated plus-maze as a measure of anxiety in the rat. *J Neurosci Methods.* 1985;14:149–67.
51. Scott JC, Matt GE, Wrocklage KM, Crnich C, Jordan J, Southwick SM, et al. A quantitative meta-analysis of neurocognitive functioning in posttraumatic stress disorder. *Psychol Bull.* 2015;141:105–40.
52. Mathew AS, Lotfi S, Bennett KP, Larsen SE, Dean C, Larson CL, et al. Association between spatial working memory and Re-experiencing symptoms in PTSD. *J Behav Ther Exp Psychiatry.* 2022;75:101714.
53. Hughes RN. The value of spontaneous alternation behavior (SAB) as a test of retention in pharmacological investigations of memory. *Neurosci Biobehav Rev.* 2004;28:497–505.
54. Henriksen EJ, Colgin LL, Barnes CA, Witter MP, Moser MB, Moser EI. Spatial representation along the proximodistal axis of CA1. *Neuron.* 2010;68:127–37.
55. Malik R, Dougherty KA, Parikh K, Byrne C, Johnston D. Mapping the electrophysiological and morphological properties of CA1 pyramidal neurons along the longitudinal hippocampal axis. *Hippocampus.* 2016;26:341–61.
56. D'Elia ATD, Juruena MF, Coimbra BM, Mello MF, Mello AF. Posttraumatic stress disorder (PTSD) and depression severity in sexually assaulted women: hypothalamic-pituitary-adrenal (HPA) axis alterations. *BMC Psychiatry.* 2021;21:174.
57. Stoppelbein L, Greening L, Fite P. The role of cortisol in PTSD among women exposed to a trauma-related stressor. *J Anxiety Disord.* 2012;26:352–8.
58. Sapolsky RM, Krey LC, McEwen BS. Stress down-regulates corticosterone receptors in a site-specific manner in the brain. *Endocrinology.* 1984;114:287–92.
59. Weidenfeld J, Feldman S, Itzik A, Van de Kar LD, Newman ME. Evidence for a mutual interaction between noradrenergic and serotonergic agonists in stimulation of ACTH and corticosterone secretion in the rat. *Brain Res.* 2002;941:113–7.
60. Reul JM, de Kloet ER. Two receptor systems for corticosterone in rat brain: microdistribution and differential occupation. *Endocrinology.* 1985;117:2505–11.
61. Karst H, Karten YJ, Reichardt HM, de Kloet ER, Schutz G, Joels M. Corticosteroid actions in hippocampus require DNA binding of glucocorticoid receptor homodimers. *Nat Neurosci.* 2000;3:977–8.
62. Chameau P, Qin Y, Spijker S, Smit AB, Joels M. Glucocorticoids specifically enhance L-type calcium current amplitude and affect calcium channel subunit expression in the mouse hippocampus. *J Neurophysiol.* 2007;97:5–14.
63. Narayanan R, Dougherty KJ, Johnston D. Calcium store depletion induces persistent perisomatic increases in the functional density of h channels in hippocampal pyramidal neurons. *Neuron.* 2010;68:921–35.
64. Santoro B, Wainger BJ, Siegelbaum SA. Regulation of HCN channel surface expression by a novel C-terminal protein-protein interaction. *J Neurosci: Off J Soc Neurosci.* 2004;24:10750–62.
65. Lewis AS, Schwartz E, Chan CS, Noam Y, Shin M, Wadman WJ, et al. Alternatively spliced isoforms of TRIP8b differentially control h channel trafficking and function. *J Neurosci: Off J Soc Neurosci.* 2009;29:6250–65.
66. Santoro B, Piskrowski RA, Pian P, Hu L, Liu H, Siegelbaum SA. TRIP8b splice variants form a family of auxiliary subunits that regulate gating and trafficking of HCN channels in the brain. *Neuron.* 2009;62:802–13.
67. Bledsoe RK, Montana VG, Stanley TB, Delves CJ, Apolito CJ, McKee DD, et al. Crystal structure of the glucocorticoid receptor ligand binding domain reveals a novel mode of receptor dimerization and coactivator recognition. *Cell.* 2002;110:93–105.
68. Ray DW, Suen CS, Brass A, Soden J, White A. Structure/function of the human glucocorticoid receptor: tyrosine 735 is important for transactivation. *Mol Endocrinol.* 1999;13:1855–63.
69. Shavit Stein E, Itsekson Hayosh Z, Vlachos A, Maggio N. Stress and Corticosteroids Modulate Muscarinic Long Term Potentiation (mLTP) in the Hippocampus. *Front Cell Neurosci.* 2017;11:299.

70. Jung-Testas I, Baulieu EE. Inhibition of glucocorticosteroid action in cultured L-929 mouse fibroblasts by RU 486, a new anti-glucocorticosteroid of high affinity for the glucocorticosteroid receptor. *Exp Cell Res.* 1983;147:177–82.
71. Choi GE, Lee SJ, Lee HJ, Ko SH, Chae CW, Han HJ. Membrane-Associated Effects of Glucocorticoid on BACE1 Upregulation and Abeta Generation: Involvement of Lipid Raft-Mediated CREB Activation. *J Neurosci.* 2017;37:8459–76.
72. Urbach V, Walsh DE, Mainprice B, Bousquet J, Harvey BJ. Rapid non-genomic inhibition of ATP-induced Cl⁻ secretion by dexamethasone in human bronchial epithelium. *J Physiol.* 2002;545:869–78.
73. Vargas G, Lucero MT. Modulation by PKA of the hyperpolarization-activated current (I_h) in cultured rat olfactory receptor neurons. *J Membr Biol.* 2002;188:115–25.
74. Kase H, Iwahashi K, Nakanishi S, Matsuda Y, Yamada K, Takahashi M, et al. K-252 compounds, novel and potent inhibitors of protein kinase C and cyclic nucleotide-dependent protein kinases. *Biochem Biophys Res Commun.* 1987;142:436–40.
75. Brackenbury WJ, Djamgoz MB. Nerve growth factor enhances voltage-gated Na⁺ channel activity and Transwell migration in Mat-LyLu rat prostate cancer cell line. *J Cell Physiol.* 2007;210:602–8.
76. Tokumitsu H, Chijiwa T, Hagiwara M, Mizutani A, Terasawa M, Hidaka H. KN-62, 1-[N,O-bis(5-isoquinolinesulfonyl)-N-methyl-L-tyrosyl]-4-phenylpiperazine, a specific inhibitor of Ca²⁺/calmodulin-dependent protein kinase II. *J Biol Chem.* 1990;265:4315–20.
77. Lu HT, Feng RQ, Tang JK, Zhou JJ, Gao F, Ren J. CaMKII/calpain interaction mediates ischemia/reperfusion injury in isolated rat hearts. *Cell Death Dis.* 2020;11:388.
78. Solomon Z, Mikulincer M. Trajectories of PTSD: a 20-year longitudinal study. *Am J Psychiatry.* 2006;163:659–66.
79. Lee KA, Vaillant GE, Torrey WC, Elder GH. A 50-year prospective study of the psychological sequelae of World War II combat. *Am J Psychiatry.* 1995;152:516–22.
80. Flurkey KCJ, Harrison DE. Mouse models in aging research. *The Mouse in Biomedical Research.* Cambridge, MA: Academic Press; 2007 pp. 637–72.
81. Olf M. Sex and gender differences in post-traumatic stress disorder: an update. *Eur J Psychotraumatol.* 2017;8:1351204.
82. DeBold JF, Miczek KA. Aggression persists after ovariectomy in female rats. *Horm Behav.* 1984;18:177–90.
83. Bremner JD, Vythilingam M, Vermetten E, Southwick SM, McGlashan T, Nazeer A, et al. MRI and PET study of deficits in hippocampal structure and function in women with childhood sexual abuse and posttraumatic stress disorder. *Am J Psychiatry.* 2003;160:924–32.
84. George MS, Abbott LF, Siegelbaum SA. HCN hyperpolarization-activated cation channels inhibit EPSPs by interactions with M-type K(+) channels. *Nat Neurosci.* 2009;12:577–84.
85. Al Abed AS, Ducourneau EG, Bouarab C, Sellami A, Marighetto A, Desmedt A. Preventing and treating PTSD-like memory by trauma contextualization. *Nat Commun.* 2020;11:4220.
86. Kaouane N, Porte Y, Vallee M, Brayda-Bruno L, Mons N, Calandreau L, et al. Glucocorticoids can induce PTSD-like memory impairments in mice. *Science.* 2012;335:1510–3.
87. Ducourneau EG, Guette C, Perrot D, Mondesir M, Mombereau C, Arnt J, et al. Brexpiprazole blocks post-traumatic stress disorder-like memory while promoting normal fear memory. *Mol Psychiatry.* 2021;26:3018–33.
88. Guidotti G, Calabrese F, Anacker C, Racagni G, Pariante CM, Riva MA. Glucocorticoid receptor and FKBP5 expression is altered following exposure to chronic stress: modulation by antidepressant treatment. *Neuropsychopharmacology.* 2013;38:616–27.
89. Robertson DA, Beattie JE, Reid IC, Balfour DJ. Regulation of corticosteroid receptors in the rat brain: the role of serotonin and stress. *Eur J Neurosci.* 2005;21:1511–20.
90. Shin M, Brager D, Jaramillo TC, Johnston D, Chetkovich DM. Mislocalization of h channel subunits underlies h channelopathy in temporal lobe epilepsy. *Neurobiol Dis.* 2008;32:26–36.
91. Ferguson JM. SSRI Antidepressant Medications: Adverse Effects and Tolerability. *Prim Care Companion J Clin Psychiatry.* 2001;3:22–27.
92. Berger W, Mendlowicz MV, Marques-Portella C, Kinrys G, Fontenelle LF, Marmar CR, et al. Pharmacologic alternatives to antidepressants in posttraumatic stress disorder: a systematic review. *Prog Neuropsychopharmacol Biol Psychiatry.* 2009;33:169–80.
93. Abdallah CG, Roache JD, Averill LA, Young-McCaughan S, Martini B, Gueorguieva R, et al. Repeated ketamine infusions for antidepressant-resistant PTSD: Methods of a multicenter, randomized, placebo-controlled clinical trial. *Contemp Clin Trials.* 2019;81:11–18.
94. Feder A, Parides MK, Murrrough JW, Perez AM, Morgan JE, Saxena S, et al. Efficacy of intravenous ketamine for treatment of chronic posttraumatic stress disorder: a randomized clinical trial. *JAMA Psychiatry.* 2014;71:681–8.
95. Chen X, Shu S, Bayliss DA. HCN1 channel subunits are a molecular substrate for hypnotic actions of ketamine. *J Neurosci: Off J Soc Neurosci.* 2009;29:600–9.
96. Anis NA, Berry SC, Burton NR, Lodge D. The dissociative anaesthetics, ketamine and phencyclidine, selectively reduce excitation of central mammalian neurones by N-methyl-aspartate. *Br J Pharm.* 1983;79:565–75.

ACKNOWLEDGEMENTS

We thank Dr. Payne Y. Chang for the behavioral software. This work was supported by Starting Fund from the Medical College of Georgia at Augusta University.

AUTHOR CONTRIBUTIONS

CSK conceived the project. CSK designed all experiments. XYL provided guidance on the chronic social defeat stress model. CSK conducted behavioral experiments, immunohistochemistry, and electrophysiology experiments. JK performed behavioral experiments, immunohistochemistry, western blotting, and neurobiotin-immuno labeling. YL performed behavioral experiments. CSK and JK analyzed data. CSK wrote the first draft of the paper. All authors read and edited the paper.

COMPETING INTERESTS

The authors declare no competing interests.

ADDITIONAL INFORMATION

Supplementary information The online version contains supplementary material available at <https://doi.org/10.1038/s41380-022-01682-9>.

Correspondence and requests for materials should be addressed to Chung Sub Kim.

Reprints and permission information is available at <http://www.nature.com/reprints>

Publisher's note Springer Nature remains neutral with regard to jurisdictional claims in published maps and institutional affiliations.



Open Access This article is licensed under a Creative Commons Attribution 4.0 International License, which permits use, sharing, adaptation, distribution and reproduction in any medium or format, as long as you give appropriate credit to the original author(s) and the source, provide a link to the Creative Commons license, and indicate if changes were made. The images or other third party material in this article are included in the article's Creative Commons license, unless indicated otherwise in a credit line to the material. If material is not included in the article's Creative Commons license and your intended use is not permitted by statutory regulation or exceeds the permitted use, you will need to obtain permission directly from the copyright holder. To view a copy of this license, visit <http://creativecommons.org/licenses/by/4.0/>.

© The Author(s) 2022